# Supplementary information

## Projected impacts of future offshore wind farms on coastal precipitation over the Northwest European shelf

Naveed Akhtar[1*], Alberto Elizalde[1], Beate Geyer[1], Corinna Schrum[1,2]
[1] Institute of Coastal Systems - Analysis and Modeling, Helmholtz-Zentrum Hereon, Geesthacht, Germany
[2] Center for Earth System Research and Sustainability, Institute of Oceanography, University of Hamburg, Germany
*Corresponding author: Naveed Akhtar (naveed.akhtar@hereon.de)

## SECTION 1

### Model horizonal and vertical resolution

### Horizontal Resolution:

The publications by Akhtar et al. (2020, 2022, 2024) were based on a ~2 km horizontal grid resolution using a smaller domain that only covered the North Sea. In this study, we selected a larger domain that includes the North Sea, the Baltic Sea, as well as the UK and Irish Sea. The reason for choosing a larger domain is to simulate a broader region, including especially the Baltic Sea and analyze the potential impact of future offshore wind farm (OWF) development. To reduce computational costs, we opted for a slightly coarser horizontal resolution. Prior to running the simulations, we conducted test studies and found that the differences in wind speed between 2 km and 5 km resolution over wind farms are minor (see Figure SI 1a, b).

**Wind speed: 5km vs 2km**

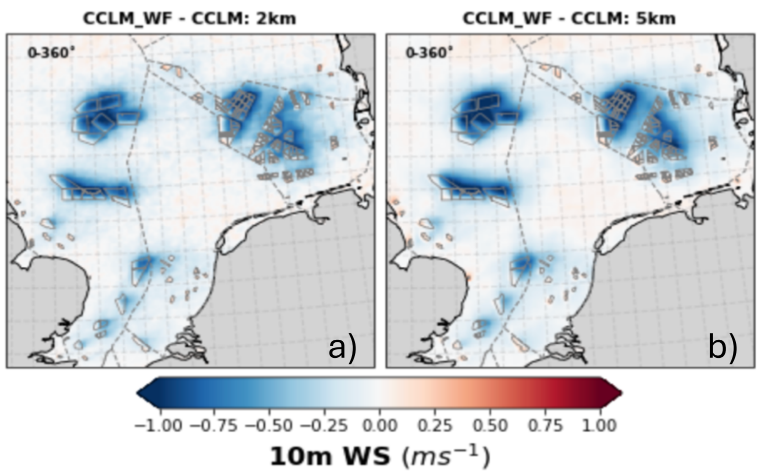


*Figure SI 1a. 10 m wind speed difference (a) CCLM_WF and CCLM with 2 km resolution and b) CCLM_WF and CCLM with 5 km resolution.*

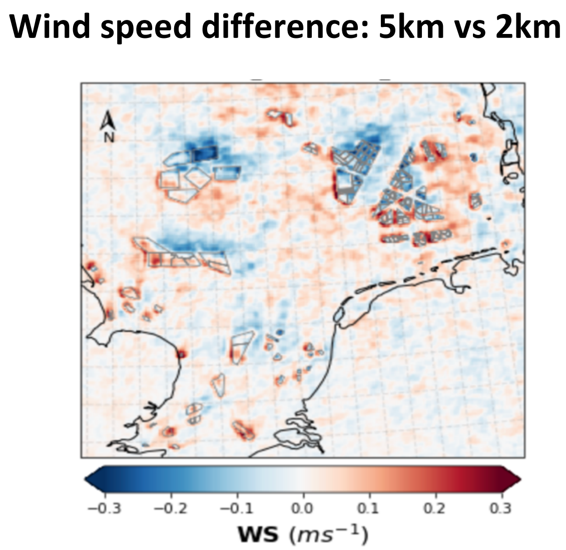


*Figure SI 1b. Difference in 10 m wind speed between COSMO-CLM simulations with wind farms at 5 km resolution (CCLM_WF05) and COSMO-CLM simulations with wind farms at 2 km resolution (CCLM_WF02).*

## Vertical resolution:

Several test simulations were carried out to identify the optimal vertical resolution: standard setup with 61 levels, two additional layers below the rotor and in the rotor area (63 levels), and standard redistributed levels for 32, 64, and 128 level (see Figure SI 2). The results indicate that differences between the various vertical resolutions are minimal over the sea, proven by analysis at the measurement platform FINO1 (Figure SI 3 and Table SI 1) and in the range of intrinsic variability of the model. However, we selected 61 vertical model levels because the wakes were better resolved over the wind farm areas, consistent with findings from an earlier study (Akhtar et al. 2021).

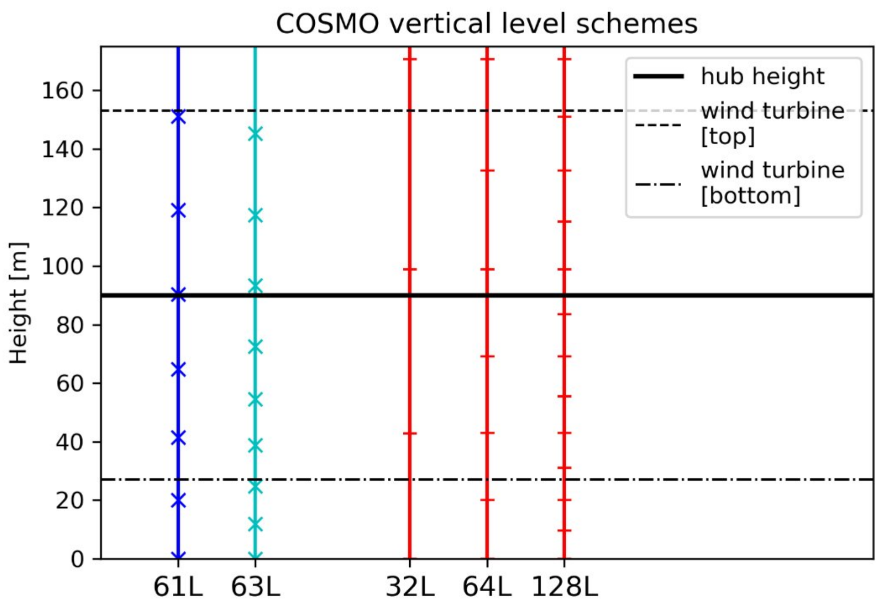


*Figure SI 2: Illustration of the location of the model layers near the Earth's surface in the test experiments: standard setup with 61 levels, two additional layers below the rotor area (63 levels), and standard redistributed levels for 32, 64, and 128 level. Crosses and ticks mark the layer boundaries; horizontal lines indicate hypothetical hub height and rotor area of a turbine. Figure was produced by Dmitrii Kovalevskii, Hereon.*

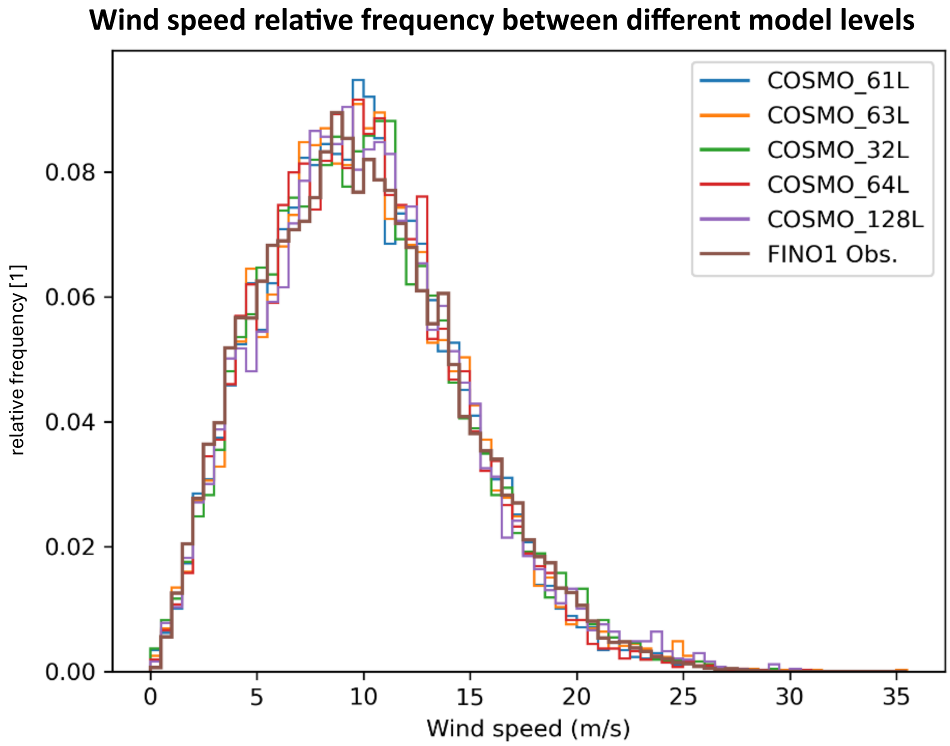


*Figure SI 3. Wind speed relative frequency on hourly basis (bin width 0.5 m/s) for comparison between COSMO-CLM simulations with different vertical resolutions and FINO1 observational data for 2008 at a height of 90.3 m. Figure was produced by Dmitrii Kovalevskii, Hereon.*

*Table SI 1: Statistical measures of observed (at 90.3 m height) and simulated wind speed data (interpolated to 90.3 m) with different setup for vertical levels at FINO1: Mean value and standard deviation [m/s], Perkin skill score, linear correlation and RMSE for the simulations compared to observational values for 2008. The standard setup with 61 levels is marked in bold. Values delivered by Dmitrii Kovalevskii, Hereon.*

| | **Observation** | **32 Level** | **61 Level** | **63 Level** | **64 Level** | **128 Level** |
|---|---|---|---|---|---|---|
| **Mean [m/s]** | 9.96 | 10.01 | **9.91** | 10.00 | 9.88 | 10.14 |
| **Std. [m/s]** | 4.67 | 4.66 | **4.49** | 4.64 | 4.47 | 4.74 |
| **PSS** | | 0.96 | **0.95** | 0.95 | 0.96 | 0.95 |
| **Linear correlation** | | 0.77 | **0.76** | 0.75 | 0.75 | 0.75 |
| **RMSE** | | 3.19 | **3.20** | 3.28 | 3.23 | 3.33 |

## SECTION 2

**Differences between technical scenarios and control simulation are replotted with either additional scenarios or a different unit.**

### Change in 10 m wind speed

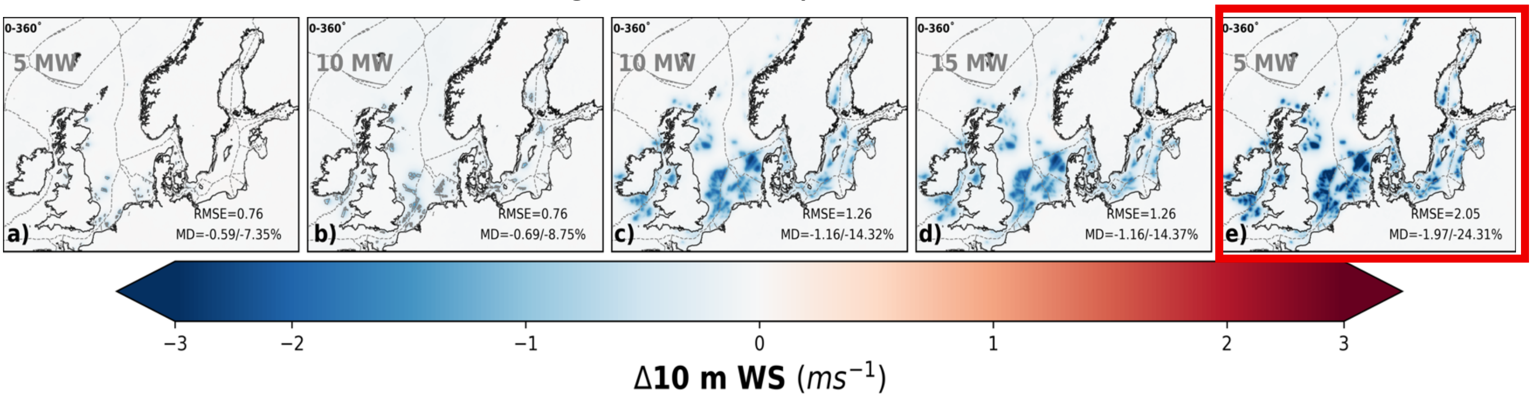


*Figure SI 4. Similar to Figure 2 in the paper but includes 5 MW turbine simulations (highlighted with a red square) for comparison*

### Change in precipitation

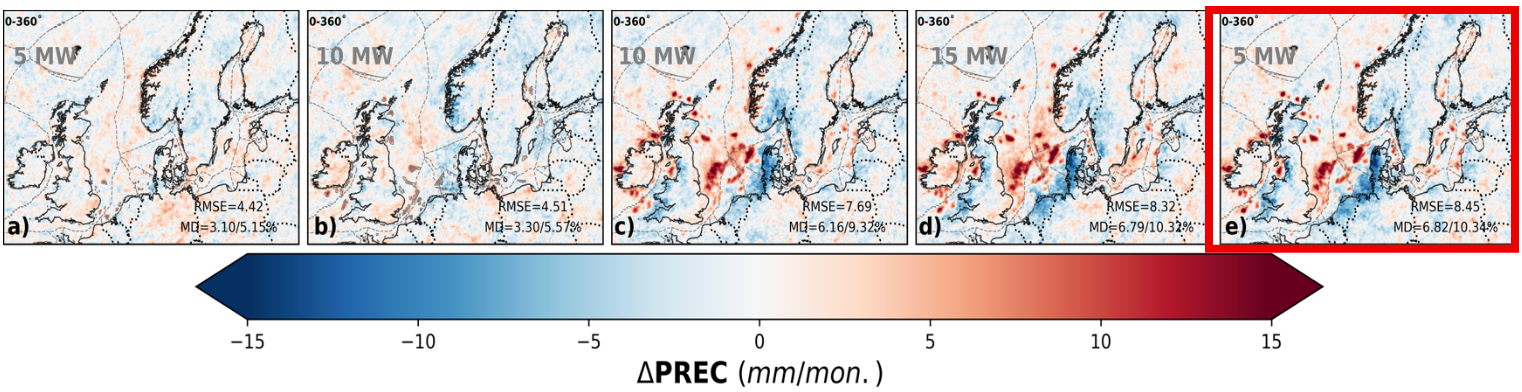


*Figure SI 5. Similar to Figure 3 in the paper, but includes 5 MW turbine simulations (highlighted with a red square) for comparison*

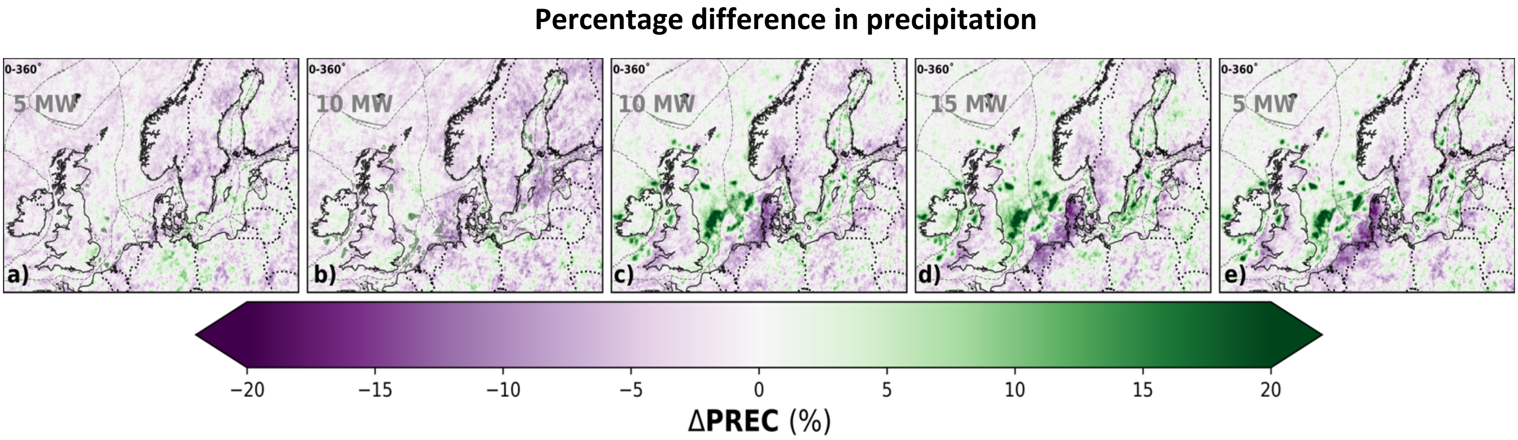


*Figure SI 6. Similar to Figure SI 4, the values are expressed as percentage differences of the absolute values*

## Statistical significances tests for precipitation

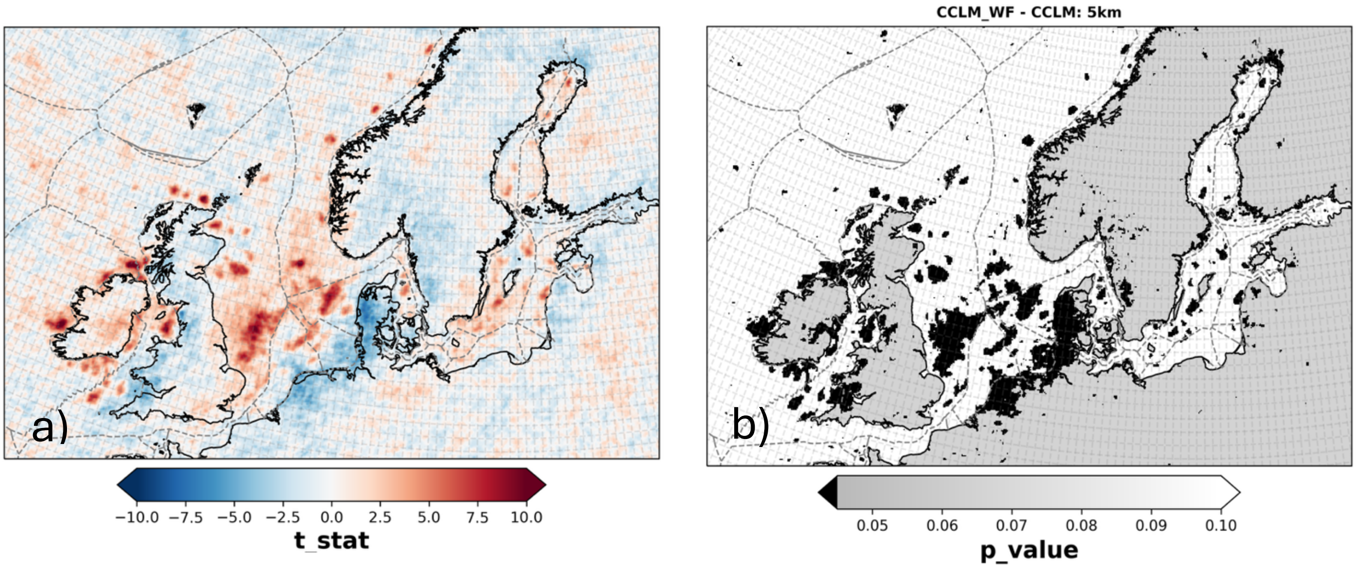


*Figure SI 7 a) t-values and b) p-values in precipitation difference between simulations with wind farms WF2050_15MW and control simulation (NOWF) for all wind directions (0—360˚) over the period of 2008—2017. This figure was created with Matplotlib ((Hunter, J. D., Matplotlib: a 2D graphics environment. Computing in Science and Engineering 9, 2007) and Cartopy (Met office, Cartopy: a cartographic python library with a matplotlib interface. Exeter, Devon, https://scitools.org.uk/cartopy, 2015).*

## Change in precipitation: over wind farm vs over land

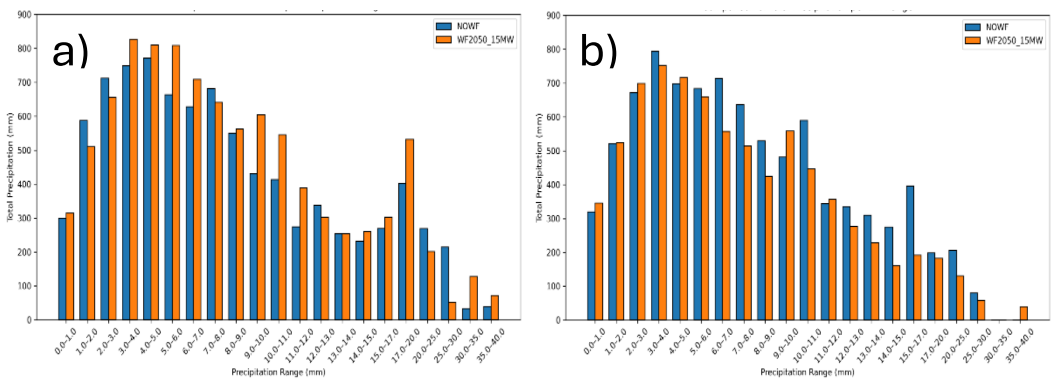


*Figure SI 8. Total precipitation amounts over bins of daily precipitation a) over wind farms in Nordsøen I subdomain and b) Jutland, Denmark subdomain of the control simulation (NOWF) and the simulation with wind farms WF2050_15MW over the period of 2008—2017. Notify the changing bin size above 15 mm per day.*

### Wind direction influence on precipitation - Dependence of precipitation changes of wind direction

In the North Sea, south-westerly winds are the dominant force[9,41]. The wind roses of simulated winds in the control simulation align well with the mast observational data from FINO1 (Fig. SI 8). The hourly simulated wind direction data over the 10-year period of 2008 to 2017 reveals that south-westerly winds (200°—280°) constitute about 33.1 % of the total wind occurrences. In comparison, the FINO1 observational data shows a similar figure of about 32.7 %. Moreover, these south-westerly winds are significantly stronger in magnitude compared to winds from other directions. Our results reveal that the reduction in precipitation around the coastal regions of Denmark, Germany, and the Netherlands mainly occurs during dominant south-westerly wind conditions (Fig. SI 9). During prevailing south-westerly wind conditions, precipitation over the wind farm increases by approximately 9—20 %, while coastal regions of Denmark, Germany, and the Netherlands experience a reduction of about 5—8 %. Under south-westerly wind conditions, the 2050 scenario simulations show an approximate increase in precipitation (MD=14.25 %) over the wind farm areas. The maximum increase is with 5 MW wind turbines, followed by 15 MW turbines (MD=14.03 %) and 10 MW turbines (MD=9.32 %). This indicates that the presence of wind farms can enhance local precipitation over the wind farm areas while simultaneously reducing it along the coast.

The impact of winds from different directions on precipitation in the coastal region varies significantly. Simulated northwesterly winds (280° to 360°) account for approximately 24 % of the total wind occurrences (also compare with Fig. SI 8 ), which is in accordance to the observations at FINO1 with about 20 %. However, winds blowing from these directions have a negligible impact on coastal precipitation (Fig. SI 4).

Winds blowing from other directions, such as those between 0° and 100° and between 100° to 200° have a negligible effect on coastal precipitation (Fig. SI 10). Although there is a slight increase in precipitation over the wind farm for 100° to 200° directions, it is not as strong as the increase for winds blowing between 200° and 280°. This suggests that the direction of the wind is a critical factor in determining precipitation patterns. South-westerly winds not only shape the weather patterns but also significantly influence the amount of rainfall in the coastal regions of Denmark, Germany, the Netherlands, and the UK.

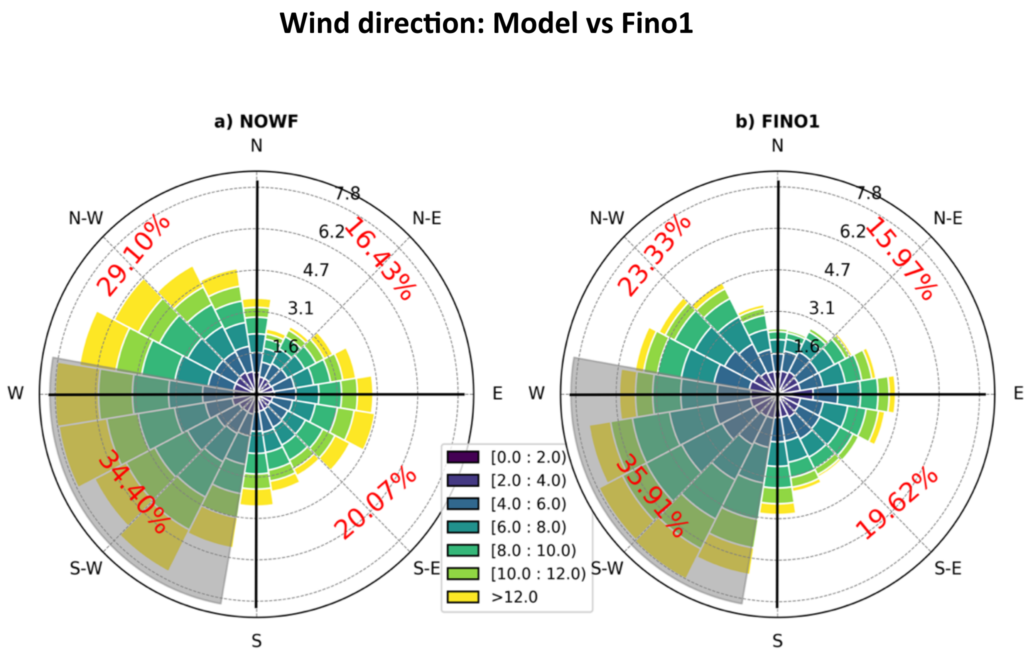


*Figure SI 9. Wind rose plot from a) control simulation (NOWF) and b) FINO1 observational data at location of research plat form FINO1 (6.5875°E, 54.01472°N). The numbers in red color indicate wind occurrence in that quadrant. The gray shaded area shows the wind directions between 200—280˚.*

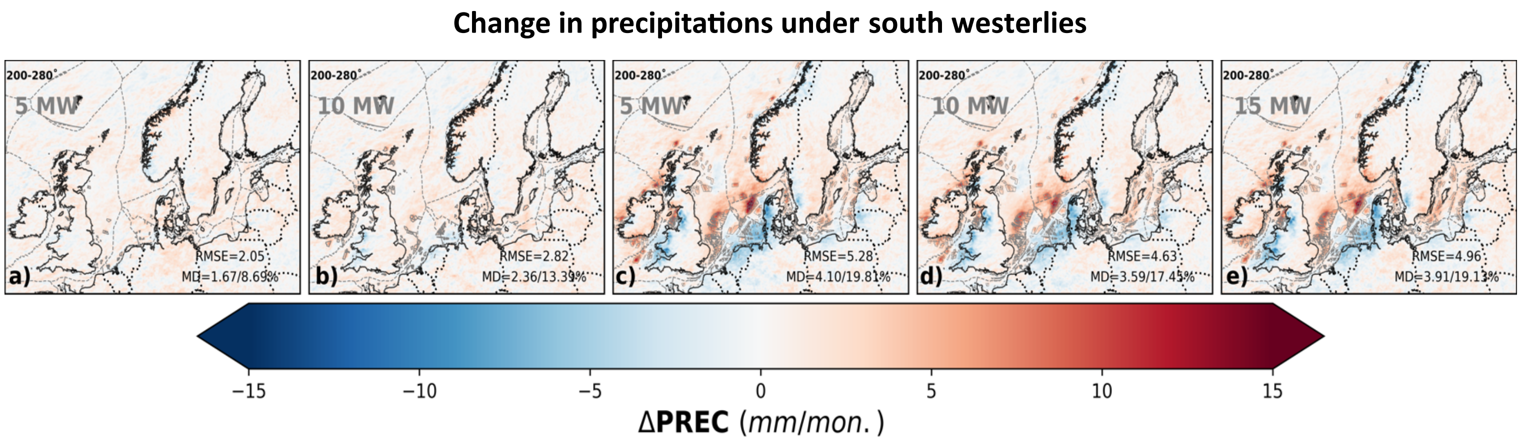


*Figure SI 10. Annual mean differences in precipitation between simulations with wind farms a) WF2023_5MW, b) WF2030_10MW, c) WF2050_5MW, d) WF2050_10MW, and d) WF2050_15MW and control NOWF simulation for wind directions from 200—280° over the period of 2008—2017. This figure was created with Matplotlib (Hunter, J. D., Matplotlib: a 2D graphics environment. Computing in Science and Engineering 9, 2007) and Cartopy (Met office, Cartopy: a cartographic python library with a matplotlib interface. Exeter, Devon, https://scitools.org.uk/cartopy, 2015).*

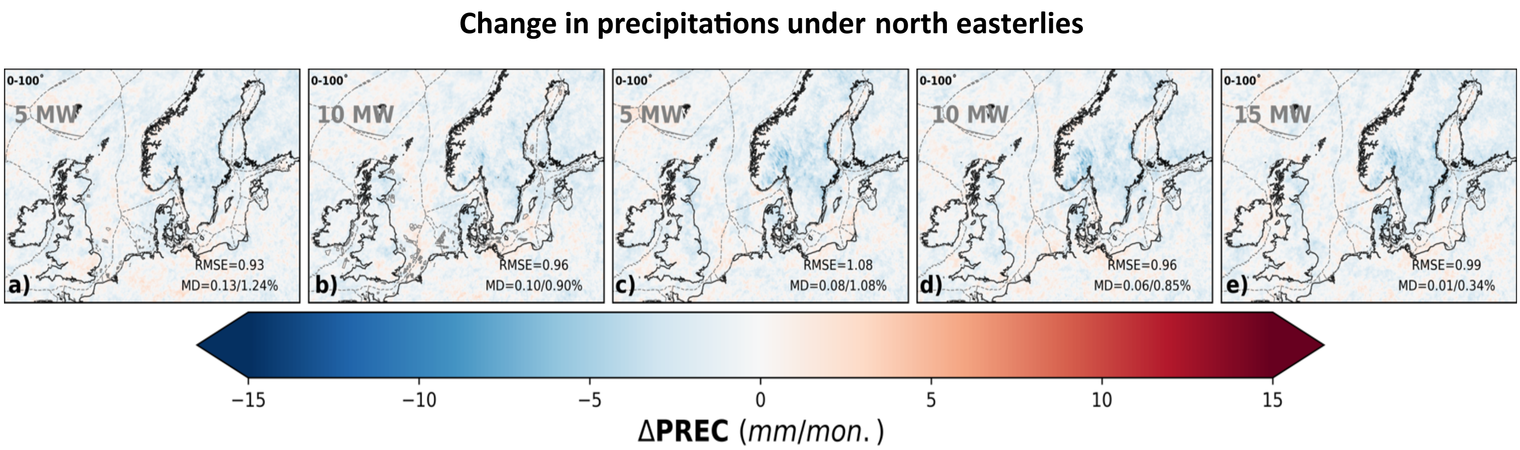


*Figure SI 11a. Annual mean differences in precipitation between simulations with wind farms a) WF2023_5MW, b) WF2030_10MW, c) WF2050_5MW, d) WF2050_10MW, and d) WF2050_15MW and control NOWF simulation for wind directions from 0—100° over the period of 2008—2017. This figure was created with Matplotlib (Hunter, J. D., Matplotlib: a 2D graphics environment. Computing in Science and Engineering 9, 2007) and Cartopy (Met office, Cartopy: a cartographic python library with a matplotlib interface. Exeter, Devon, https://scitools.org.uk/cartopy, 2015).*

**Change in precipitations under south easterlies**

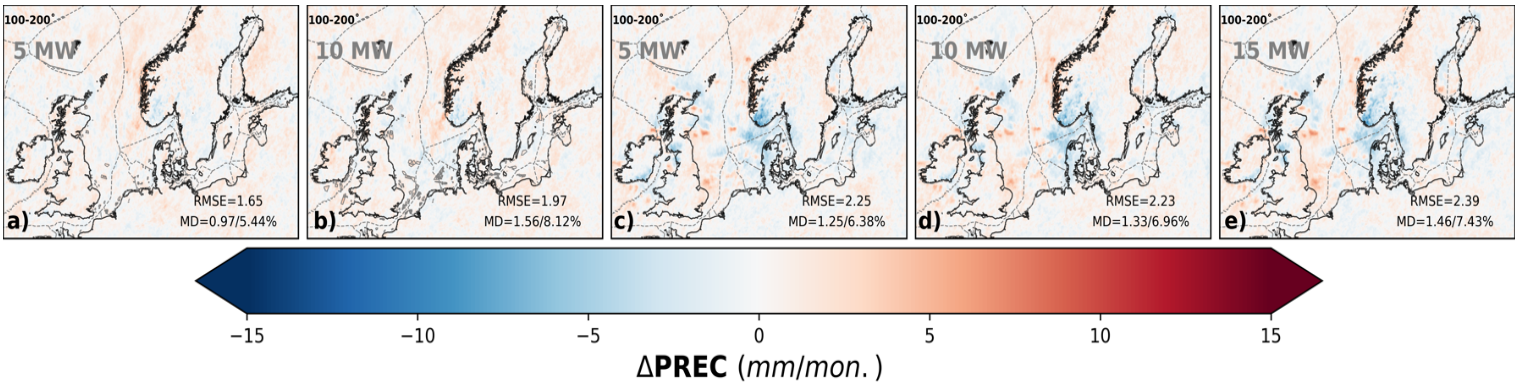


*Figure SI 11b. Same as Fig. SI 11a but for wind directions from 100-200˚.*

**Change in precipitations under north westerlies**

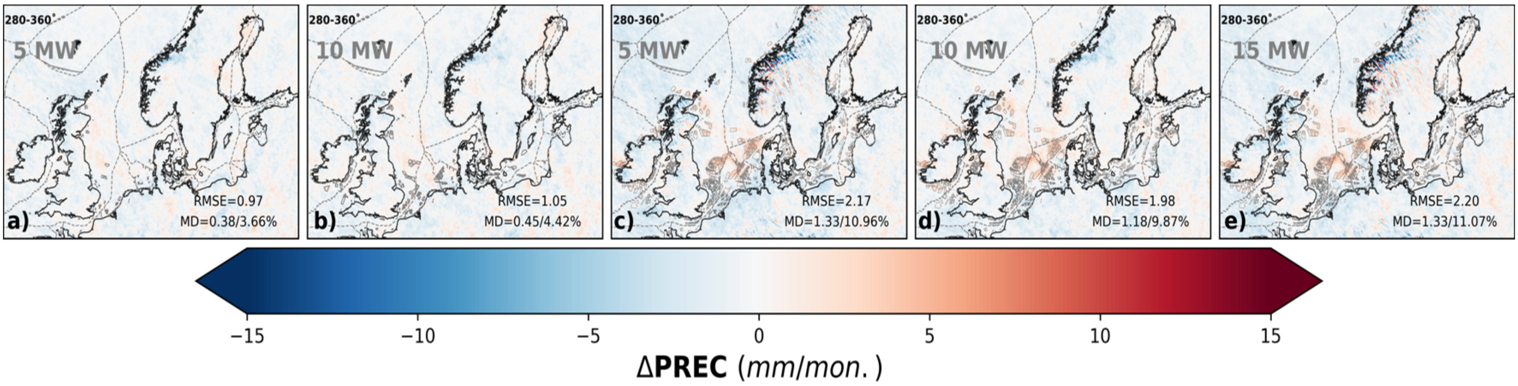


*Figure SI 11c. Same as Fig. SI 11a but for wind directions from 280-360˚.*

**Seasonal impact on precipitation**

On seasonal timescales, the reduction in coastal precipitation in all 2050 scenarios is more pronounced, except during spring, compared to the control simulations (see e.g., Fig. SI 12a-c). During winter and autumn, south-westerly winds (200—280˚) dominate the North Sea, accounting for 38 % and 34 % of the total wind occurrences, respectively (Fig. SI 13). In contrast, during spring and summer, north-westerly winds prevail, with 25 % and 31 % of the total wind occurrences, respectively. Indicating that these winds serve as the primary source of moisture transport from the sea to the land. In winter and autumn not only the direction of the south-westerly winds are dominating but also the magnitude of the wind speed is higher than spring and summer. The seasonal mean differences of other simulations in comparison to control simulations are shown in SI (Fig. SI 12).

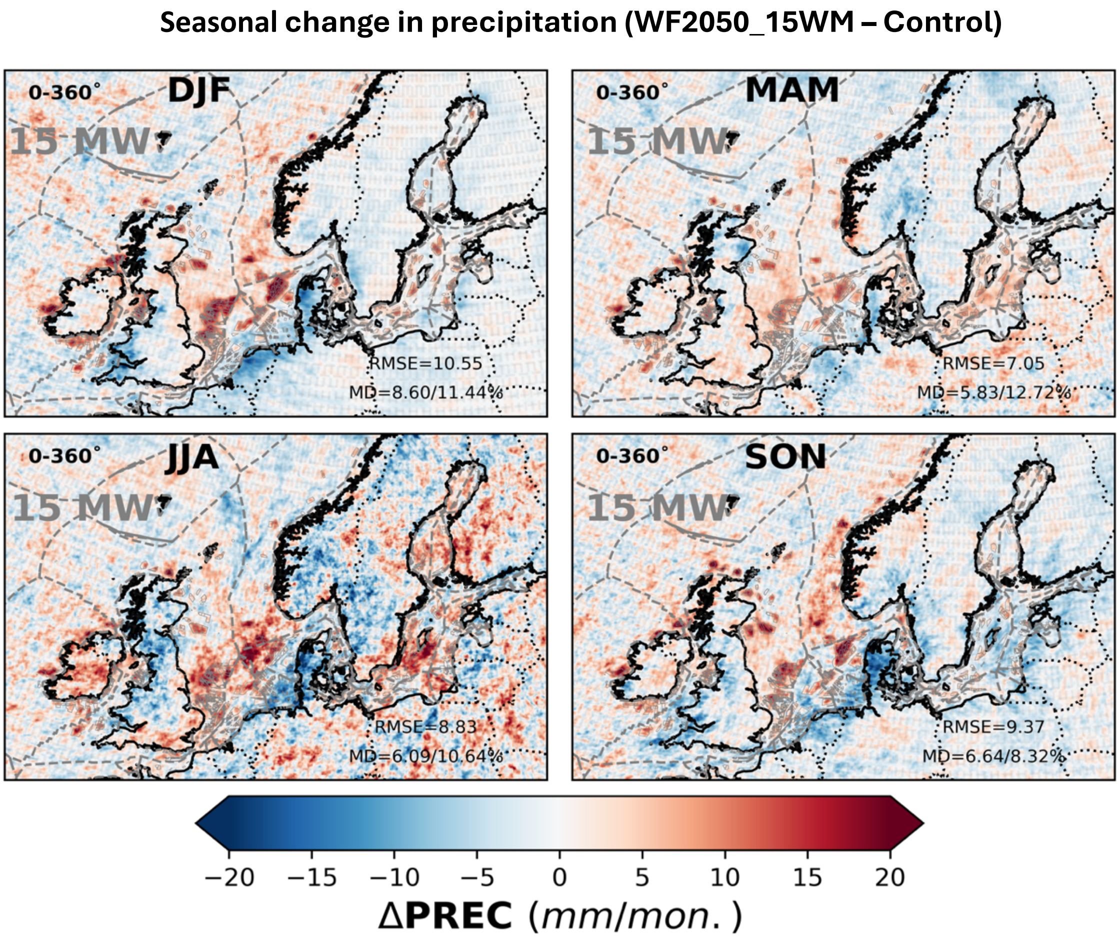


*Figure SI 12a. Seasonal mean differences in precipitation between the simulation with wind farms WF2050_15MW and control simulation (NOWF) for all wind directions (0—360˚) over the period of 2008—2017. This figure was created with Matplotlib (Hunter, J. D., Matplotlib: a 2D graphics environment. Computing in Science and Engineering 9, 2007) and Cartopy (Met office, Cartopy: a cartographic python library with a matplotlib interface. Exeter, Devon, https://scitools.org.uk/cartopy, 2015).*

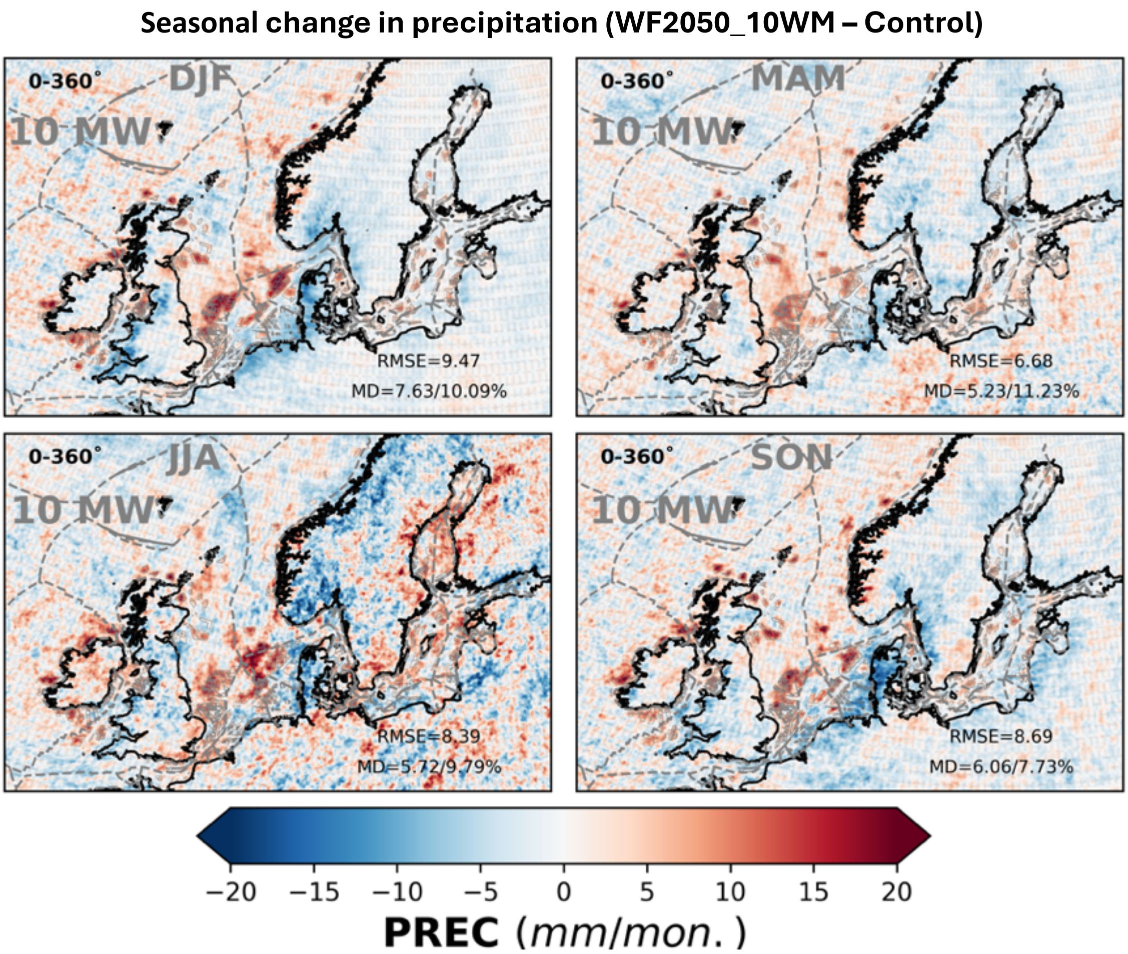


*Figure SI 12b. Same as Fig. SI 12a but for WF2050_10MW.*

**Seasonal change in precipitation (WF2050_5WM – Control)**

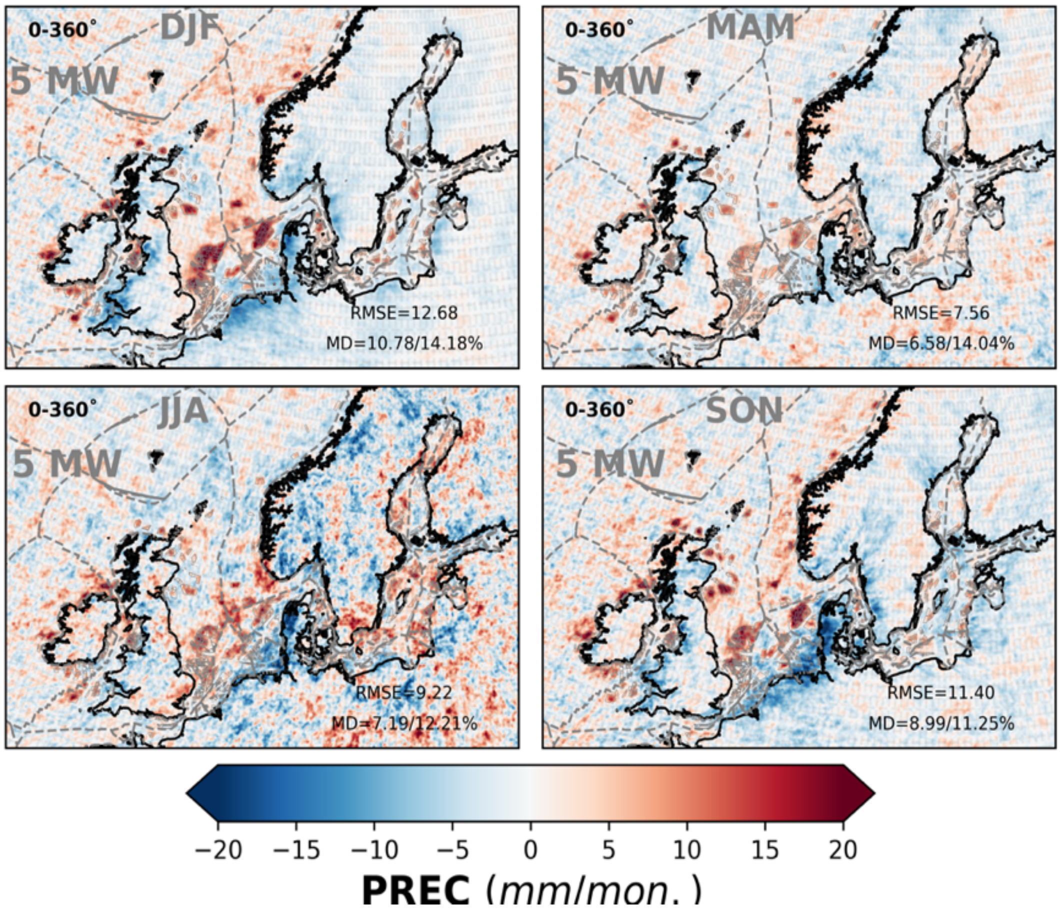


*Figure SI 12c. Same as Fig. SI 12a but for WF2050_5MW.*

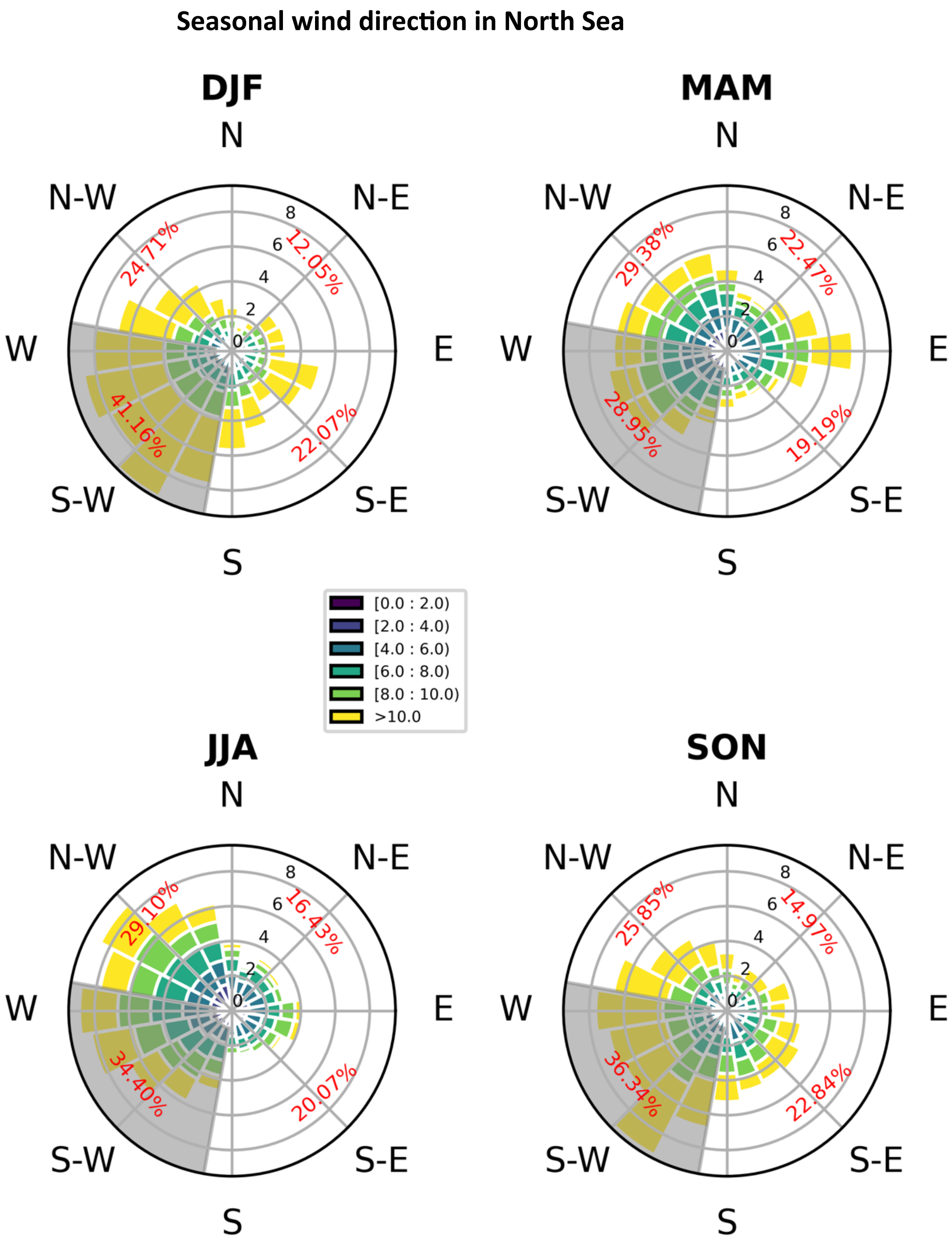


*Figure SI 13. Seasonal wind rose plot from control simulation NOWF for winter (DJF), spring (MAM), summer (JJA), and autumn (SON) at location of research plat form FINO1 (6.5875°E, 54.01472°N). The numbers in red color indicate wind occurance in that quadrant. The gray shaded area shows the wind directions between 200—280˚.*

**Wind speed influence on precipitation**

The magnitude of the simulated wind speed shows good agreement with the observed data from the FINO1 mast station. The simulated wind speed in the control simulation at FINO1 indicates that approximately 59.5 % of the winds range between 3 and 12 $ms^{-1}$, while around 35 % fall between 12 and 25 $ms^{-1}$. Our results show good agreement with the observations at FINO1, with values of approximately 60.5 % and 30.8 %, respectively. The slightly lower numbers at FINO1 are primarily due to the construction of wind farms in the surrounding area. Our results show that the increase in precipitation over the wind farm is higher when the wind speed falls between 12 and 25 $ms^{-1}$. However, the reduction in precipitation over the land is more significant when the wind speed ranges between 3 and 12 $ms^{-1}$ (Fig. SI 14). Wind farms are considered as inoperative at wind speeds below 3 $ms^{-1}$ and above 25 $ms^{-1}$, resulting in no observed changes in wind speed and precipitation over the wind farms during these conditions.

**Change in precipitation field under different wind speeds**

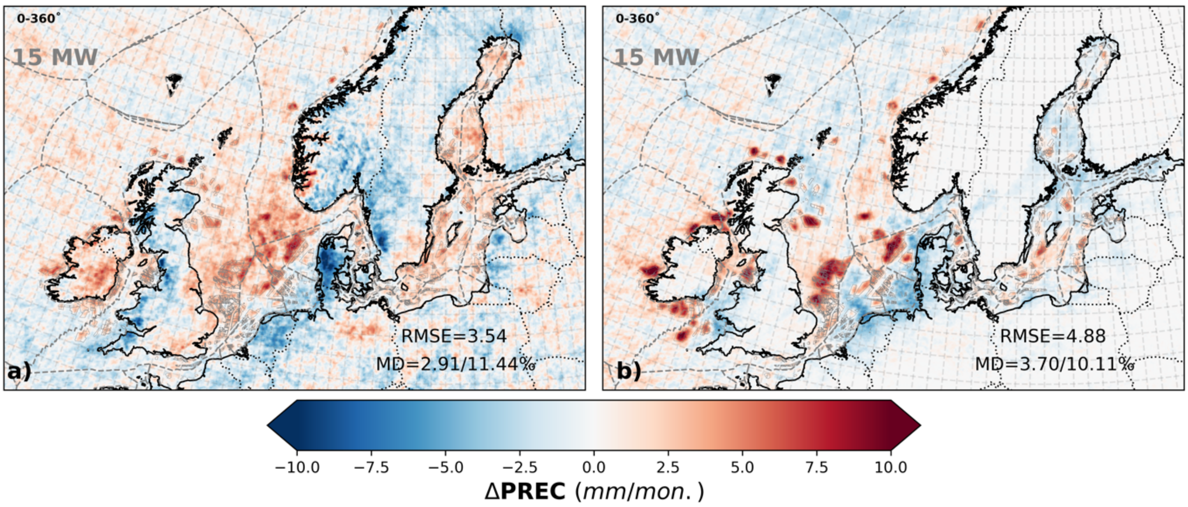


*Figure SI 14. Annual mean differences in precipitation between simulations with wind farms WF2050_15MW and control simulation (NOWF) for wind speeds between a) 3 to 12 $ms^{-1}$, and b) 12 to 25 $ms^{-1}$for all wind directions (0—360˚) over the period of 2008—2017. This figure was created with Matplotlib (Hunter, J. D., Matplotlib: a 2D graphics environment. Computing in Science and Engineering 9, 2007) and Cartopy (Met office, Cartopy: a cartographic python library with a matplotlib interface. Exeter, Devon, https://scitools.org.uk/cartopy, 2015).*

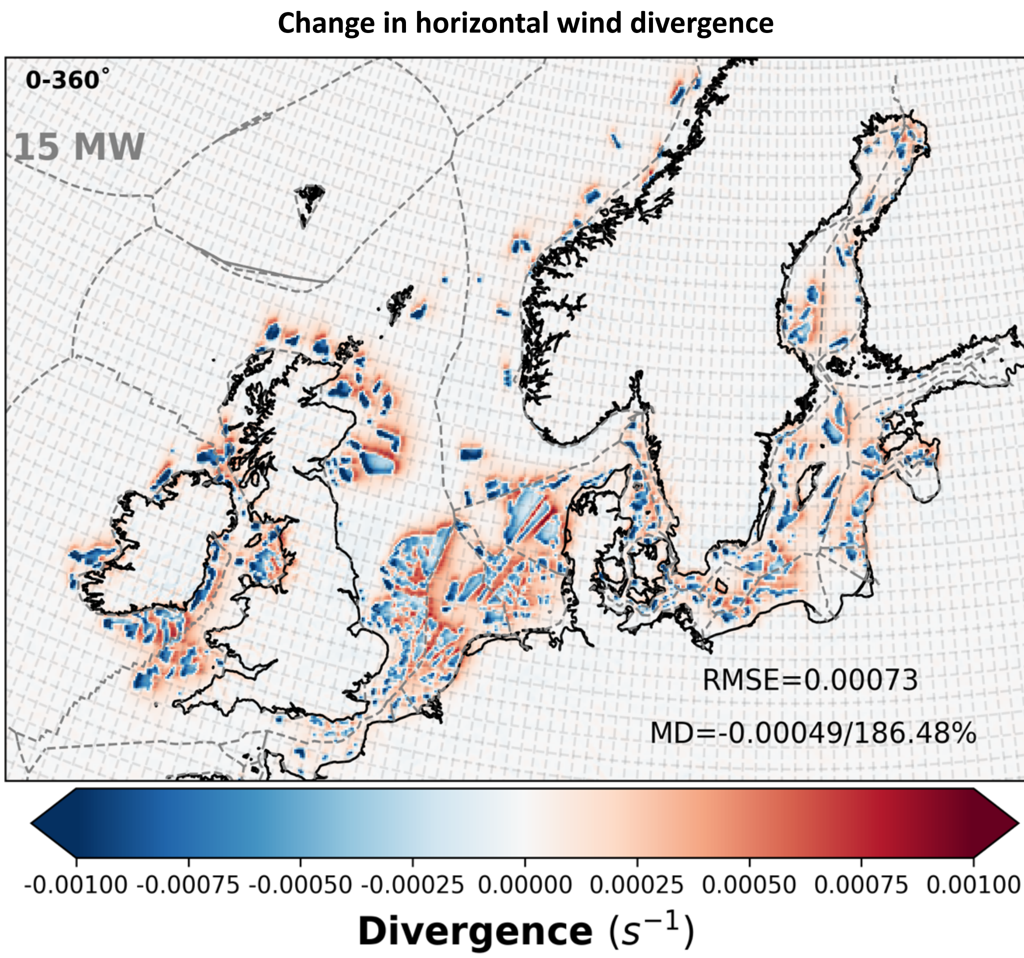


*Figure SI 15. Annual mean differences in horizontal wind divergence between simulations with wind farms WF2050_15MW and control simulation (NOWF) for all wind directions (0—360°) over the period of 2008—2017. This figure was created with Matplotlib (Hunter, J. D., Matplotlib: a 2D graphics environment. Computing in Science and Engineering 9, 2007) and Cartopy (Met office, Cartopy: a cartographic python library with a matplotlib interface. Exeter, Devon, https://scitools.org.uk/cartopy, 2015).*

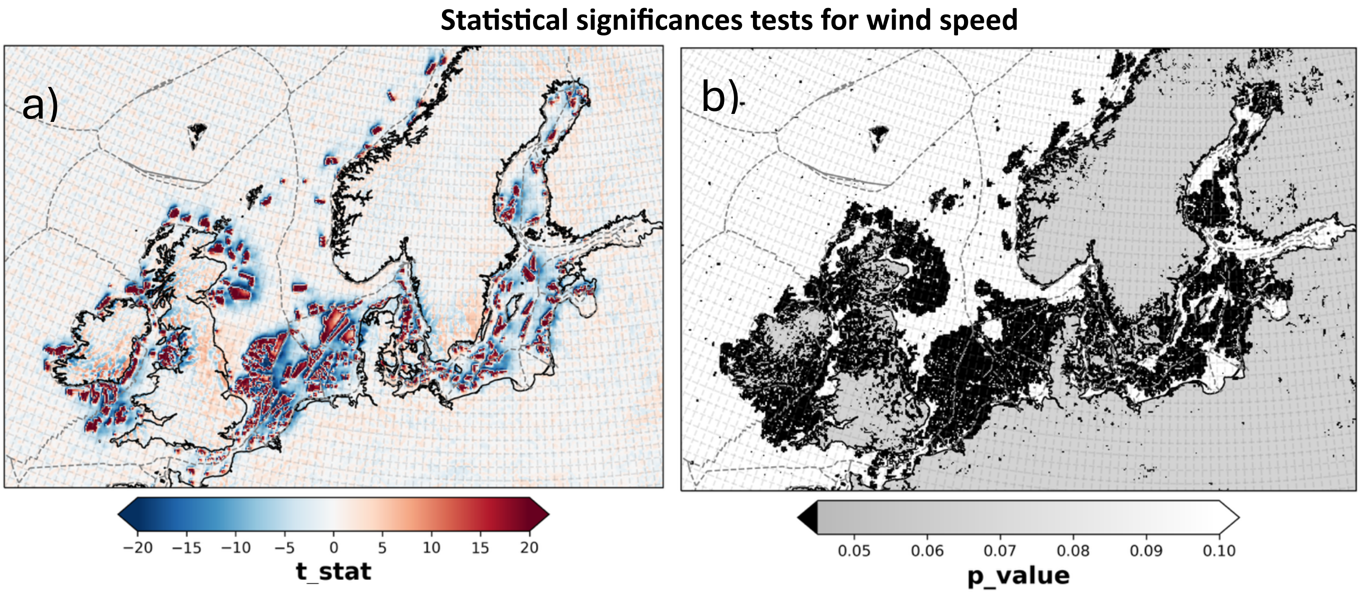


*Figure SI 16. a) t-values and b) p values in horizontal wind difference between simulations with wind farms WF2050_15MW and control simulation (NOWF) for all wind directions (0—360˚) over the period of 2008—2017. This figure was created with Matplotlib (Hunter, J. D., Matplotlib: a 2D graphics environment. Computing in Science and Engineering 9, 2007) and Cartopy (Met office, Cartopy: a cartographic python library with a matplotlib interface. Exeter, Devon, https://scitools.org.uk/cartopy, 2015).*

# Reference:


Akhtar, N., Geyer, B. & Schrum, C. Impacts of accelerating deployment of offshore windfarms on near-surface climate. *Sci. Rep.* **12**, 18307 (2022).

Akhtar, N., Geyer, B. & Schrum, C. Larger wind turbines as a solution to reduce environmental impacts. *Sci. Rep.* **14**, 1–12 (2024).

Akhtar, N., Geyer, B., Rockel, B., Sommer, P. & Schrum, C. Accelerating deployment of offshore wind energy alter wind climate and reduce future power generation potentials. In review. *Sci. Rep.* 2021 (2021) doi:10.1038/s41598-021-91283-3.

Borgers, R. *et al.* Mesoscale modelling of North Sea wind resources with COSMO-CLM: model evaluation and impact assessment of future wind farm characteristics on cluster-scale wake losses. *Wind Energy Science* **9**, 697–719 (2024).

Elizalde, A., Akhtar, N., Geyer, B. & Schrum, C. Uncertainty in Offshore Wind Power Forecasts: A Regional Climate Modeling Approach for the North Sea. Preprint at https://doi.org/10.5194/wes-2025-64 (2025).

Früh, B. (2023). *Aktualisierung der Datengrundlage für die Anpassung an den Klimawandel in Deutschland*. https://www.dwd.de/DE/forschung/projekte/udag/udag_node.htm

Geyer, B. High-resolution atmospheric reconstruction for Europe 1948–2012: coastDat2. *Earth Syst. Sci. Data* **6**, 14–164 (2014).

Rockel, B., Will, A. & Hense, A. The regional climate model COSMO-CLM (CCLM). *Meteorologische Zeitschrift* **17**, 347–348 (2008).